Available online at www.sciencedirect.com

Manufacturing Letters

Manufacturing Letters 00 (2024) 000–000

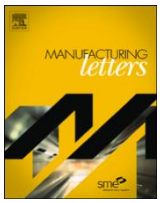

52nd SME North American Manufacturing Research Conference (NAMRC 52, 2024)

Hybrid manufacturing cost models: Additive friction stir deposition, measurement, and CNC machining

Nathan Wilson[a], Robert Patterson[a], Elijah Charles[a], Malachi Landis[b], Joshua Kincaid[a], Ryan Garcia[a], Gregory Corson[a], Tony Schmitz[a,c*]

[a]*University of Tenneessee, Knoxville, 1512 Middle Drive, Knoxville, TN 37996, USA*
[b]*Northwestern University, 2145 Sheridan Rd., Evanston, IL, 60208, United States of America*
[c]*Oak Ridge National Laboratory, Manufacturing Demonstration Facility, 2350 Cherahala Blvd., Knoxville, TN 37932, USA*

* Corresponding author. Tel.: +1-865-974-6141. *E-mail address:* tony.schmitz@utk.edu.

Abstract

Based on its potential to reduce lead times, hybrid manufacturing, which often includes both additive manufacturing and machining processes, is receiving more attention from manufacturers as they seek to increase their supply chain resilience and efficiency. A new solid-state additive manufacturing, referred to as additive friction stir deposition, has shown the potential to become an important process for hybrid manufacturing. To justify selection of a hybrid manufacturing approach, the cost need to be estimated for comparison to conventional approaches. Historically, hybrid manufacturing costs have been difficult to estimate due to the complexity and diversity of the manufacturing processes. This paper proposes cost models that include additive friction stir deposition, structured light scanning, milling, and turning, which can be combined in hybrid manufacturing process planning. These cost models are demonstrated in a case study and cost estimates are compared for hybrid and conventional (machining-only) manufacturing approaches. The results of the case study show that both labor and material costs must be considered to make an informed decision between hybrid and conventional manufacturing approaches.

Keywords: Hybrid manufacturing, cost, additive friction stir deposition, metrology, machining

1. Introduction

With increased attention paid to supply chain resilience globally, reducing lead times is becoming progressively more important [1]. Greater focus has been placed on hybrid manufacturing processes as a potential solution for reducing costs related to lead times as well as improving supply chain efficiency and agility [2]. In this context, hybrid manufacturing represents a combination of two or more conventional manufacturing processes [3]. Due to the large number of manufacturing processes, it can be difficult to accurately estimate part production cost without access to process-specific cost models for all manufacturing processes included in the hybrid manufacturing plan.

This paper provides cost models for a hybrid manufacturing sequence that includes additive friction stir deposition (AFSD), measurement of the preform using structured light scanning (SLS), and machining operations. The paper is organized as follows. First, the cost models are described. Second, the models are implemented using a case study with a manufacturing sequence that includes AFSD, SLS, milling, and turning for a selected part geometry. Third, a discussion of the results is provided.

The accurate calculation of production costs is vital to the success of manufacturing companies [4]. There are various

methods and models that are available. Examples include traditional cost modeling, activity-based cost modeling (ABC), and parametric cost modeling [5]. For hybrid manufacturing, activity-based and parametric cost modeling are well-suited to describing and predicting the costs incurred by part production [6]. Parametric cost modeling uses statistical methods to evaluate the relationship between inputs including part size, volume, material type, and production cost. It identifies which variables most affect production cost [4]. ABC modeling, on the other hand, considers the process and process physics [7]. This paper develops cost models using the ABC approach.

ABC was introduced to address the difficulty of attributing indirect costs to individual parts [8]. Traditional costing methods only evaluate direct labor and materials costs. ABC accounts for both direct and indirect costs in part production [9]. As noted, ABC is process-dependent and relies on the physics of each manufacturing process to predict the corresponding costs more accurately [7]. ABC makes it possible to attribute indirect costs to each part produced.

Managerial accounting is chiefly concerned with gathering information needed for decision-making [10]. In contrast to financial accounting, which is focused on creating financial reports for people outside the organization, managerial accounting is intended for internal use. Because the cost models presented here are useful for internal decision-making, principles from managerial accounting were applied. In managerial accounting, there is a difference between product costs and period costs. Product costs are those directly related to production. This could include material, labor, facility rental, and utilities, for example. Period costs are those that do not directly apply to production, such as insurance, marketing, sales, and salaries of support personnel, for example. The focus of this paper is estimating the cost to make a specific part using hybrid manufacturing. Because period costs do not contribute directly to part production costs, they are not considered here.

Production costs are divided into two categories: direct costs and indirect costs. Direct costs are defined as any cost that can be directly traced. Examples include material and labor costs since these values are exactly known. In contrast, indirect costs are classified as those that are not conveniently traceable, but still contribute to the overall manufacturing cost for a selected part. Examples include space use, energy use, depreciation, and maintenance. Not only are these costs challenging to quantify for each part, but they are also subjective, particularly for depreciation and maintenance [11]. The exact depreciation cannot be known but can still represent a significant cost [6].

As stated, hybrid manufacturing is any combination of two or more manufacturing processes to produce a single part [3]. The processes can be separated into additive and machining (subtractive) categories [12], where their combination can reduce lead times and improve supply chain efficiency [13]. Additive manufacturing processes, such as AFSD, wire arc additive manufacturing (WAAM), powder bed fusion (PBF), and fused filament fabrication (FFF), increase manufacturing agility and flexibility by producing complex geometries without dies, molds, or tooling [12][14]. Additive processes can also be more energy efficient and reduce material use relative to traditional manufacturing processes [15]. Subtractive manufacturing, such as CNC milling and turning, complements these processes by achieving the surface finish and part tolerances that additive processes cannot match, in general [16]. Prior research has shown that additive and machining processes can be used in a variety of combinations [14][17][18][19]. In some instances, measurements are incorporated into hybrid manufacturing processes [19], which improves process efficiency by the addition of metrology to enable coordinate systems transfer between additive and machining processes [18][20][21][22]. Additionally, measurements can be used to assess the part quality [23].

AFSD is a solid-state metal additive manufacturing technique first developed by Schultz and Creehan [24]. At that time, it was known as friction stir fabrication. AFSD publications appeared in 2009 with the dissertation of Gray [25], followed by an introductory paper by Schultz and Creehan in 2013 [26] and a thesis by Calvert in 2015 [27]. The pace of publication increased after 2017 following the first peer-reviewed article on AFSD microstructure by Rivera [28]. A related AFSD process has also been reported [29].

AFSD builds on prior deposition and welding techniques, such as friction surfacing (FS) and friction stir welding (FSW) [30]. In AFSD, a rotating shoulder applies torque to a square feedstock rod which is pressed against a substrate [31]. Friction between the feedstock and the substrate causes heating, typically to 60% to 90% of the feedstock melt temperature, at which point the feedstock begins to flow into a gap between the substrate and the base of the tool shoulder. Further friction between the base of the shoulder and the feedstock causes feedstock-substrate mixing and additional heating. A deposition track is formed as the deposition head traverses across the substrate. AFSD machines provided by MELD Manufacturing (an L3 was applied in this study) use feedstock sizes on the order of 10 mm square and 300 mm in length, producing approximately 40 mm wide depositions [32]. Typical shoulder rotation rates are between 200 rpm and 1000 rpm, layer thicknesses are a few millimeters or less, and traverse and feedstock feed rates approximately 1 mm/s [33].

As a solid-state method, AFSD presents unique differences to melt-based techniques, such as directed energy deposition (DED) and laser power bed fusion (LPBF). These rely on the melting and solidification of metal powders to form parts. The associated phase change can produce defects such as cracking and porosity [34][35]. AFSD avoids such solidification problems, enabling the printing of non-weldable alloys. A wide variety of metals have been successfully deposited by AFSD. Aluminum is the most common with demonstrations of 2024 [36], 2050 [37], 2219 [38], 5083 [39], 6061 [40], 6063 [41], 7020 [42], 7050 [43], and 7075 [44] alloys. Magnesium alloys AZ31B [45] and WE43 [46] have been deposited. Pure copper [47], 110 Cu [48], Inconel 625 [49], and stainless steels 304 [50], 316 [33], and 316L [51] have also been demonstrated. There are opportunities for metal matrix composites (MMC) enabled by the inherent mixing within the process as demonstrated with nanodiamonds [52], graphene nanoplatelets [53], and silicon carbide [54].

While still a developing technology, there is growing interest in large scale production using AFSD. For example, the Jointless Hull Program has constructed the largest metal 3D printer in the world with AFSD as the enabling technology [55]. Widespread use of AFSD within industry will require

economic justification and, therefore, cost modelling. The intent of this paper is to add the required cost models to the literature.

2. Cost models

The goal for hybrid manufacturing cost models is to accurately predict costs on a part-by-part basis. Because hybrid manufacturing is flexible by nature, the cost models must also be flexible to best accommodate the various manufacturing process combinations. Each of the process models stand alone and may be used in any combination or order to estimate cost for the selected hybrid manufacturing process sequence.

The cost model structure includes both direct and indirect costs; see Eqs. 1-3, where the total cost can be decreased when recycling cost recovery is available. Direct costs are divided into material, labor, energy, and tool costs. It's important to note that energy costs are typically classified as indirect costs because they can be difficult to quantify. However, since energy consumption measurements are becoming more common (current measurement to determine power, for example), energy use is classified as a direct cost in this study. Additionally, tool costs and recycling cost recover are only included in the subtractive process cost models. Indirect costs include contributions from depreciation, maintenance, and space use.

$$Total\ costs = Direct\ costs + Indirect\ costs - Recycling\ cost\ recovery \quad (1)$$

$$Direct\ costs = Material\ costs + Labor\ costs + Energy\ costs + Tool\ costs \quad (2)$$

$$Indirect\ costs = Depreciation\ costs + Maintenance\ costs + Space\ costs \quad (3)$$

Each manufacturing process has a cost model following this general format. Because the processes differ, formulas unique to each process are included. Cost models for AFSD, SLS, turning, and milling are provided in the following sections.

2.1 AFSD cost model

The AFSD cost model includes the total build cost, C_{build}, the direct build cost, $C_{b,dir}$, and the indirect build cost, $C_{b,ind}$. See Eqs. 4-6.

$$C_{build} = C_{b,dir} + C_{b,\ ind} \quad (4)$$

$$C_{b,dir} = C_{mat} + C_{lab} + C_{enr} \quad (5)$$

$$C_{b,ind} = C_{space} + C_{dep} + C_{maint} \quad (6)$$

The direct build costs include material costs, C_{mat}, labor costs, C_{lab}, and energy costs, C_{enr}. Indirect costs include space costs C_{space}, depreciation costs, C_{dep}, and maintenance costs, C_{maint}. See Eqs. 7-10.

$$C_{mat} = (n_{bar} \cdot c_{bar}) + c_{baseplate} + c_{gas} \quad (7)$$

$$n_{bar} = \frac{V_{part}}{V_{bar}} \quad (8)$$

$$V_{bar} = A_{bar} \cdot L_{bar} \quad (9)$$

$$c_{gas} = \frac{t_{print} \cdot F \cdot V_{tnk} \cdot c_g}{L_{tnk}} \quad (10)$$

Material costs include the deposited material, the baseplate, and the cover gas; see Eq. 7, where the deposited material cost is the number of feedstock bars, n_{bar}, multiplied by the cost per bar, c_{bar}. If the number of feedstock bars is not provided by the program generating the deposition paths, n_{bar} can be estimated by dividing the part volume, V_{part}, by the bar volume, V_{bar}, which is determined from the product of its cross-sectional area and length. The baseplate cost, $c_{baseplate}$, is its purchase price, although it may be reused multiple times. For estimating cover gas costs, c_{gas}, t_{print} represents print (deposition) time, F is a correction factor used to account for simplifications that may be applied for time estimates (such as infinite acceleration of machine axes), V_{tnk} is the gas cannister volume, c_g is the cost of the cover gas per unit volume, and L_{tnk} is the average time a full gas tank will last based on the expected application rate. Note that cover gas is not required for all alloys systems. When it is not required, c_{gas} is zero.

$$C_{lab} = (t_{setup} + t_{sup}) \cdot r_{lab} \quad (11)$$

Labor costs include setup time, t_{setup}, and supervision time, t_{sup}. The sum of these times is multiplied by the labor wage rate, r_{lab}, as shown in Eq. 11. Supervision time is typically the same as print time. Depending on the amount of attention the machine requires, however, the two variables may differ. This equation neglects the time to generate the part program that defines the machine motions during deposition. Because part program generation is a one-time cost, it applies only to the first part produced. The associated programming labor cost can be prorated over the number of parts produced. In that case, the Eq. 11 labor cost model can be updated.

$$C_{enr} = t_{print} \cdot F \cdot c_{enr-rate} \cdot r_{enr} \quad (12)$$

The energy cost, C_{enr}, in Eq. 12 includes $c_{enr\text{-}rate}$, which represents the cost per unit of electricity ($/kW-hr, for example) and r_{enr} represents the rate of energy usage (kW-hr, for example).

Space cost is estimated in Eq. 13, where $U_{space,mat}$ represents the space used by the stored material, $U_{space,mach}$ is the space used by the machine, $c_{space,fix}$ is the fixed cost of the space, and $p_{space,fix}$ is the period of the fixed space payments in units of time. In Eqs. 14-16, $c_{equi,i}$ represents initial cost of the equipment (or machine), v_{sal} is the amount the machine could be sold for at the end of its useful life (salvage value), and L_{exp} is the life expectancy of the machine. Depreciation cost is calculated using the straight-line depreciation method.

$$C_{space} = \frac{c_{space,fix}}{p_{space,fix}} \cdot t_{print} \cdot F \cdot \frac{(U_{space,mach} + U_{space,mat})}{U_{space,tot}} \quad (13)$$

$$C_{dpr} = t_{print} \cdot F \cdot \frac{(c_{equ,i} - v_{sal})}{L_{exp}} \quad (14)$$

$$C_{maint} = \frac{c_{maint}}{L_{maint}} \cdot t_{print} \cdot F \quad (15)$$

Maintenance costs are typically incurred over a set time period. To allocate these costs on a per part basis the accrued maintenance cost, c_{maint}, is divided by the time it took to accrue this cost, L_{maint}. Multiplying this by the print time and time correction factor assigns a portion of the costs to that part. See

Eq. 15.

2.2 SLS cost model

The structured light scanning (SLS) cost, C_{SLS}, is separated into direct, $C_{SLS,dir}$, and indirect, $C_{SLS,ind}$, costs. See Eqs. 16-18.

$$C_{SLS} = C_{SLS,dir} + C_{SLS,ind} \tag{16}$$
$$C_{SLS,dir} = C_{mat} + C_{lab} + C_{enr} \tag{17}$$
$$C_{SLS,ind} = C_{space} + C_{dpr} + C_{maint} \tag{18}$$

Material costs for SLS are comprised of the number, n_{stick}, and cost of stickers, c_{stick}, that are often used to serve as fiducials that connect one image to the next in the instrument software, as well as the amount of spray that is often used to reduce reflectively and increase image quality; see Eq. 19 The spray mass, m_{spray}, can be calculated by weighing the spray container before and after the SLS process. Alternately, the mass can be calculated using the part surface area, A_{part}, volume of spray it takes to cover a unit area, V_{spray}, and the spray density, r_{spray}. SLS labor costs include setup time, t_{setup}, scan time, t_{scan}, the number of scans, n_{scan}, time spent analysing and adjusting the digital model, $t_{analysis}$, cleaning time to remove the spray coating, t_{clean}, and the labor wage rate as shown in Eq. 21. The energy cost is calculated using Eq. 22.

$$C_{mat} = n_{stick} \cdot c_{stick} + m_{spray} \cdot c_{spray} \tag{19}$$
$$m_{spray} = A_{part} \cdot V_{spray} \cdot \rho_{spray} \tag{20}$$
$$C_{lab} = \left(t_{setup} + t_{scan} \cdot n_{scan} + t_{analysis} + t_{clean} \right) \cdot r_{lab} \tag{21}$$
$$C_{enr} = r_{enr} \cdot c_{enr-rate} \cdot t_{scan} \cdot n_{scan} \tag{22}$$

SLS depreciation and maintenance costs are calculated using Eqs. 14-15, substituting total scanning time ($t_{scan} \cdot n_{scan}$) for t_{print}. The SLS space cost is calculated using Eq. 23.

$$C_{space} = \frac{c_{space,fix}}{p_{space,fix}} \cdot t_{scan} \cdot n_{scan} \cdot \frac{U_{space,mach}}{U_{space,tot}} \tag{23}$$

2.3 Machining cost model

Milling and turning have similar cost models; see Eqs. 24-26. Both are included because hybrid manufacturing applications may include both processes [22].

$$C_x = C_{x,dir} + C_{x,ind} - P_{recy} \tag{24}$$
$$C_{x,dir} = C_{mat} + C_{tool} + C_{lab} + C_{enr} \tag{25}$$
$$C_{x,ind} = C_{space} + C_{dpr} + C_{maint} \tag{26}$$

In Eq. 24, C_x denotes the total cost where either *mill* or *turn* can be inserted in place of x. The same x substitution applies for $C_{x,dir}$ (direct costs) or $C_{x,ind}$ (indirect costs). Tool cost, C_{tool}, and recycling cost recovery, P_{recy}, if applicable, are included in Eqs. 24 and 25. C_{mat} is the purchase cost of the workpiece material when the workpiece is not created by additive manufacturing in Eq. 25. If the workpiece was created using additive manufacturing, its cost is calculated using another model and C_{mat} is zero for the machining cost calculation.

$$C_{tool} = \frac{\left(t_{ch} \cdot r_{lab} + c_{tool} \right) \cdot t_x \cdot F}{T} \tag{27}$$
$$T(milling) = C \cdot v^{-n} \cdot f_t^{-p} \cdot b^{-q} \tag{28}$$
$$T(turning) = C \cdot v^{-p} \cdot f_r^{-q} \tag{29}$$

Tool cost is unique to each machining processes. It is estimated in Eq. 27 by dividing the total cost of replacing a tool by the tool life. The time to change the tool, t_{ch}, labor wage rate, and the initial purchase price of each tool used, c_{tool}, which may be greater than one for a large part with significant material removal, make up the tool changing cost. Multiplying this sum by machining time, t_x, and the time adjustment factor, and dividing by the Taylor-type tool life, T, gives the total tool cost. The tool life may be estimated using Eq. 28 for milling and Eq. 29 for turning. In these equations, v is the cutting speed, f_t is the feed per tooth, b is the axial depth of cut, f_r is the feed per revolution, and C, p, and q are constants that depend on the material-tool-process combination [56].

$$MRR(miling) = a_{mill} \cdot b \cdot f_t \cdot m \cdot N \tag{30}$$
$$MRR(turning) = v \cdot a_{turn} \cdot f_r \tag{31}$$

The mean material removal rate, MRR, is shown in Eq. 30 for milling and Eq. 31 for turning. This describes the volume of material removed per unit time. In these equations, a_{mill} is the radial depth of cut, b is the axial depth of cut, m is the number of teeth, N is the spindle speed, and a_{turn} is the turning depth of cut.

$$t_x = \frac{V_{rem}}{MRR} \tag{32}$$

The machining time can be estimated using the computer aided manufacturing (CAM) software. If this time is not available, Eq. 32 can be applied, where V_{rem} is the volume of material to be removed.

$$C_{enr} = r_{enr} \cdot c_{enr-rate} \tag{33}$$
$$r_{enr} = K_s \cdot MRR \cdot t_x \cdot F \tag{34}$$

When the rate of energy usage cannot be measured, it can be estimated using Eq. 34, where K_s is the specific cutting force. This estimation is approximate since MRR varies with the machining parameters, which vary during a selected part program, and there are other electrical components within the machine that also consume energy. Equations 33-34 are applicable to both milling and turning.

$$C_{lab} = \left(t_{setup} + t_x \cdot F \right) \cdot r_{lab} \tag{35}$$

The labor cost is calculated using Eq. 35 and applies to both machining processes. As mentioned previously, the time spent programming the cutting paths has been omitted.

$$C_{space} = \frac{c_{space,fix}}{p_{space,fix}} \cdot t_x \cdot F \cdot \frac{U_{space,mach}}{U_{space,tot}} \tag{36}$$

Space cost is calculated reusing variables from Eq. 13, substituting t_x for t_{print}. For the remaining indirect costs (maintenance and depreciation) use Eqs. 14-15, again

substituting t_x for t_{print}.

$$P_{recy} = -m_{mat,rem} \cdot p_{coll} \cdot r_{sell} \quad (37)$$

$$m_{mat,rem} = -V_{rem} \cdot \rho_{mat,rem} \quad (38)$$

Some manufacturing facilities collect and recycle metal chips produced by the machining processes. Cost recovery from these efforts, P_{recy}, is calculated using the mass removed, $m_{mat,rem}$, the percent of the material that is reclaimed, p_{coll}, and the price per mass at which it can be sold, r_{sell}. If the mass of the material to be removed is not readily available, it can be estimated using the volume and density, $\rho_{mat,rem}$, of the material removed. Equations 37-38 apply to both turning and milling processes.

3. Case study

A hexagon-cylinder geometry (see Fig. 1) was selected as the case study subject since its hybrid manufacturing process sequence includes AFSD, SLS, three-axis CNC milling, and two-axis CNC turning. It can also be made using three-axis milling only, which provides a cost comparison for evaluating the potential benefits of hybrid manufacturing process. For this case study, a physical part was produced using hybrid manufacturing methods and digital tool paths were created for three-axis milling the part from wrought stock to provide a cost comparison.

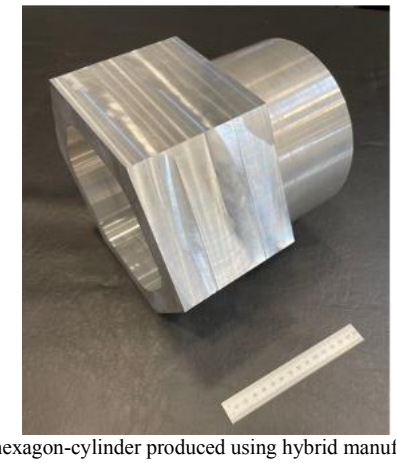

Fig. 1. The hexagon-cylinder produced using hybrid manufacturing (AFSD, SLS, milling, and turning) with a 150 mm (5.9”) machinist scale.

For the hybrid manufacturing process, the hexagon-cylinder is made from 6061-T6 aluminum bars deposited by AFSD. The corresponding preform geometry was measured using SLS to enable machining tool paths to be generated using CAM software. Both milling and turning were applied to achieve the final part dimensions. This section details the manufacturing process and application of the cost models. A description of the tool paths and application of the milling cost model for the milling-only solution is also provided.

3.1 Hybrid manufacturing

3.1.1 AFSD

AFSD of the hexagon-cylinder geometry implemented alternating deposition and machining steps in a two-sided strategy. The hexagon was first deposited on one side of the baseplate. After scanning, the hexagon was then machined, including the incorporation of the baseplate into the part. It was then inverted for the subsequent cylinder deposition on the bottom of the hexagon (the other side of the original baseplate). After the cylinder deposition and scanning, turning was used to obtain the final cylinder geometry and surface finish.

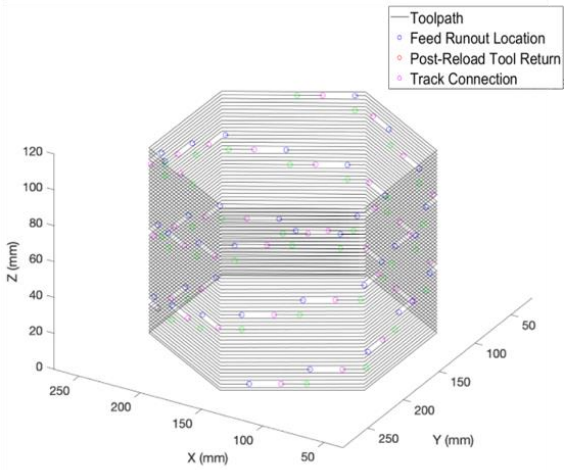

Fig. 2. Toolpaths with feedstock reload locations are shown for the hexagon.

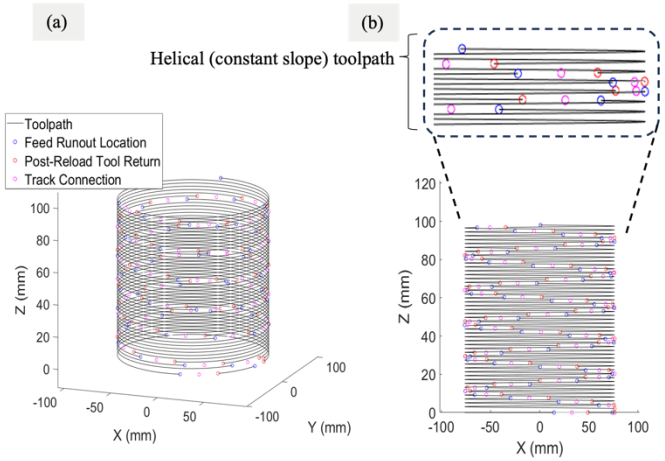

Fig. 3. Toolpaths and feedstock reload locations are shown for the (a) cylinder with (b) an expanded view.

Two AFSD part programs were required. These were programmed manually using MATLAB™. Because the MELD Manufacturing L3 machine used a discrete feed approach where each feedstock bar was individually loaded during deposition, parameterized codes were developed to use commanded material and tool feed rates to automatically track material use along individual toolpaths for the hexagon and cylinder. This identified stopping locations throughout each toolpath where feedstock reloading was completed. Once reload locations were identified, appropriate reload cycles were inserted into the part program. Hexagonal and circular toolpaths were helically interpolated at a constant slope to minimize process transients and flash accumulation associated with abrupt layer changes. Examples of deposition stop and restart locations as well as the helical toolpaths are shown in Figs. 2 and 3.

For the AFSD process, wrought 6061-T6 aluminum bars (9.5 mm × 9.5 mm × 508 mm) were used. The 6061-T6 aluminum baseplate dimensions were 304.8 mm × 304.8 mm × 25.4 mm. A flat shouldered H-13 steel tool with 9.5 mm by 9.5 mm square cross section bore for feedstock deposition was selected. The deposition initiation routine following each feedstock reload was operator guided. Each time plastic flow of the feedstock was reached, and steady-state deposition ensued, machine control was transferred to the machine controller. In the hexagon part programs, the first layer spindle speed was 300 rpm, while the spindle speed was 160 rpm for all subsequent layers (due to heat accumulation). The material feed rate was 139. 7 mm/min, and the tool feed rate was 132.1 mm/min. In the cylinder part program, the first layer spindle speed was 275 rpm, while the spindle speed was 115 rpm for all subsequent layers. The same material and tool feed rates as the hexagon deposition were commanded.

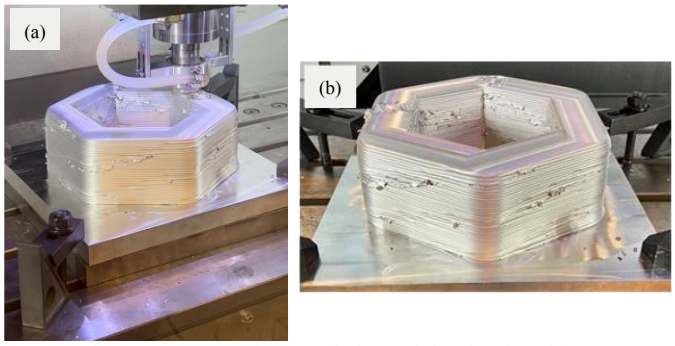

Fig. 4. Hexagon preform (a) during and (b) after deposition.

The hexagon preform was completed by aligning the baseplate with the machine table, clamping the baseplate to the table using four toe clamps, and then locating the work coordinate system at the substrate's top corner using an edge finder attached to the machine spindle. The hexagon preform was then deposited by interpolating a single-track deposit along a toolpath that increased by a constant increment with each completed perimeter, producing non-planar layers with a constant 2 mm layer height. This approach was followed until the desired preform build height was reached. Photographs of the hexagon deposition are displayed in Fig. 4.

The preform was removed from the AFSD machine and scanned. This scan was imported into the CAM software and the origin was set at the baseplate corner with coordinate directions aligned to the baseplate sides. The tool paths were generated using this coordinate system. The preform was then transferred to a three-axis CNC milling machine (Haas VF-4) and standard probing routines were used to align the machine coordinate system to the baseplate and part program coordinate system. The hexagon preform was then machined using face milling and contouring operations.

After machining the hexagon, the cylinder deposition was completed by returning the part back to the AFSD machine. For the second side deposition, the part was inverted and clamped in a vise using the hexagon flats. The spindle-mounted edge finder was used to locate the hexagon center and the work coordinate system was set at this location. The cylinder was then deposited using this coordinate system. A helical path was followed to reduce process transients while maintaining a layer height of 2 mm. The deposition process is shown in Fig. 5. The cylinder was built to a height sufficient to completely contain the final part geometry.

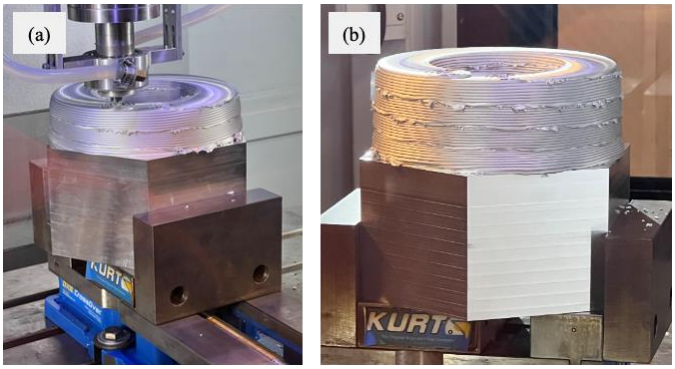

Fig. 5. The cylinder preform is displayed (a) during and (b) after deposition.

The hexagon side of the preform required 39 bars (approximately 4.89 kg of aluminum). The hexagon deposition time was 4.2 hours. For the cylinder side, 29 bars were required (approximately 3.64 kg of aluminum). The deposition time for the cylinder was 3.6 hours. This includes a 4-minute reload cycle for each bar.

Table 1. AFSD cost model variables, values, and units for the hexagon-cylinder.

Variable	Value	Units
n_{bar}	68	-
c_{bar}	1.59	$
$c_{baseplate}$	110.65	$
c_{gas}	-	$/m^3
t_{setup}	18	min
t_{sup}	469	min
r_{lab}	40	$/hr
t_{print}	469	min
F	1	-
$c_{enr\text{-}rate}$	0.12	$/kWh
r_{enr}	7	kW
$c_{space,fix}$	75,000	$
$p_{space,fix}$	1	yr
$U_{space,mach}$	46.82	m^2
$U_{space,mat}$	4.45	m^2
$U_{space,tot}$	1393	m^2
$c_{equi,i}$	600,000	$
v_{sal}	0	$
L_{exp}	10	yr
$c_{maint,p}$	0	$
$c_{maint,t}$	8,203	$
$l_{maint,p}$	0	-
$l_{maint,l}$	1	yr

To populate the AFSD cost model, the parameters in Table 1 were applied. The deposition times and material use for both depositions were combined into a single value to calculate a total AFSD cost for the hexagon-cylinder. The resulting AFSD cost estimate is $613.32. A summary is provided in Table 2.

Table 2. AFSD cost model summary.

Cost	Value
Direct build costs	**$550.00**
Material cost	$218.77
Labor cost	$324.66
Energy cost	$6.57
Indirect build costs	**$63.32**
Space cost	$2.46
Depreciation cost	$53.54
Maintenance cost	$7.32
Total cost	**$613.32**

3.1.2 SLS

In this study, a GOM ATOS Q scanner and GOM Inspect professional software were used to create scans of the part geometry after each deposition. A scan of the AFSD preform was aligned with the desired CAD geometry using an automated best fit algorithm within the GOM Inspect software. See Fig. 6. Once aligned, a coordinate system was assigned to the preform for machining tool path generation. Based on the process plan, two scans were required: one after the first deposition (hexagon) and another after the second deposition (cylinder). Additional details are provided in Dvorak et al. [19].

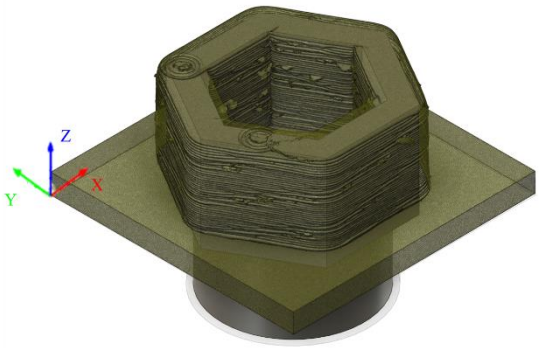

Fig. 6. A structured light scan of the hexagon preform (deposited on a baseplate) was aligned to the CAD model to define the machining coordinate system.

Like the AFSD cost model, totals from both SLS operations were combined to calculate the SLS cost. The values are provided in Table 3. Applying Eqs. 16-23 resulted in the total SLS cost of $175.33. Labor is a large fraction of this cost as seen in Table 4.

Table 3. SLS cost model variables, values, and units for the hexagon-cylinder.

Variable	Value	Units
n_{stick}	53+33	-
c_{stick}	0.11	$
m_{spray}	200	g
c_{spray}	0.0875	$/g
$t_{setup,SLS}$	60	min
t_{scan}	0.5	min
n_{scan}	33+45	-
$t_{analysis}$	60	min
t_{clean}	60	min
r_{lab}	40	$/hr
$c_{enr\text{-}rate}$	0.3	kW
r_{enr}	0.12	$/kWh
$c_{space,fix}$	75,000	$
$p_{space,fix}$	1	yr
$U_{space,mach}$	18.95	m^2
$U_{space,tot}$	1393	m^2
$c_{equi,i}$	70,000	$
v_{sal}	0	$
L_{exp}	8	yr
$c_{maint,p}$	0	$
$c_{maint,t}$	0	$
$l_{maint,p}$	0	-
$l_{maint,}$	0	yr

Table 4. SLS cost model summary.

Cost	Value
Direct build costs	**$172.98**
Material cost	$26.96
Labor cost	$146.00
Energy cost	$0.02
Indirect build costs	**$2.35**
Space cost	$0.76
Depreciation cost	$2.28
Maintenance cost	$0.00
Total cost	**$175.33**

3.1.3 Milling

All three-axis CNC milling operations used a 76.2 mm diameter face mill (Kennametal M4D300L 1108S 100L 175). The operating parameters were: 5115 rpm spindle speed, 3302 mm/min roughing feed rate, and 1397 mm/min finishing feed rate. The milling operations included: 1) facing the hexagon's top surface; and 2) contouring of the exterior and interior preform sidewalls to the finished hexapod dimensions. The hexagon was then inverted, and the milling operations included: 1) facing the exposed surface of the baseplate; and 2) contouring the baseplate edges to match the hexagon outer dimensions. Toolpaths for both operations are shown in Fig. 7. Special consideration was taken to ensure the hexagon of the first operation aligned with the second by milling in the side of the build plate slightly in the first operation and probing this milled section once the part was inverted. The machining sequence is shown in Fig. 8.

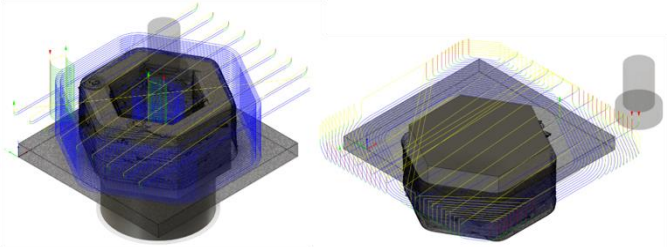

Fig. 7. Machining toolpaths for (left) hexagon and (right) baseplate after inverting the part.

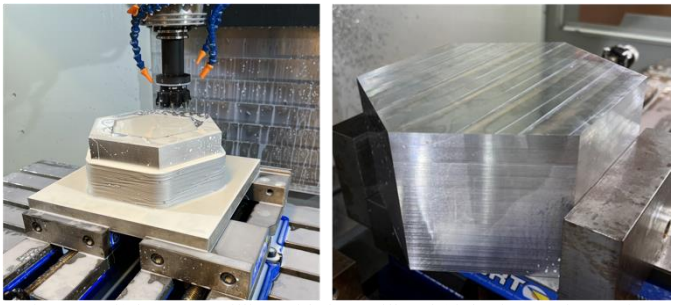

Fig. 8. (Left) hexagon milling with face mill and (right) inverted part after milling was complete.

Table 5. Milling cost model variables, values, and units for the hexagon-cylinder (produced by hybrid manufacturing).

Variable	Value	Units
C_{mat}	0	$
c_{tool}	300	$
t_{ch}	10	min
C	17,500	-
v	1224	m/min
n	0.025	-
p	0.015	-
f_t	0.122	mm/min
q	0.015	-
V_{rem}	-	mm^3
a	63.5	mm
b	25	mm

m	4	teeth
N	5115 rpm	rpm
t_{setup}	30 min	min
t_{sup}	35	min
r_{lab}	40	$/hr
t_{mill}	35	min
F	1.5	-
$c_{enr\text{-}rate}$	0.12	$/kWh
r_{enr}	15.5	kW
$c_{space,fix}$	75,000	$
$p_{space,fix}$	1	yr
$U_{space,mach}$	24.71	m^2
$U_{space,tot}$	1393	m^2
$c_{equi,i}$	78,295	$
v_{sal}	0	$
L_{exp}	10	yr
$c_{maint,p}$	0	$
$c_{maint,t}$	2,500	$
$l_{maint,p}$	0	-
$l_{maint,l}$	1	yr
p_{coll}	0	%

The values for the milling cost model are provided in Table 5. The resulting cost estimate for milling the hexagon portion of the part is $58.90. Again, labor is the largest cost. The cost summary is shown in Table 6.

Table 6. Milling cost model summary.

Cost	Value
Direct build costs	**$57.74**
Stock material cost	$0.00
Tool cost	$1.11
Labor cost	$55.00
Energy cost	$1.63
Indirect build costs	**$2.35**
Space cost	$0.13
Depreciation cost	$0.78
Maintenance cost	$0.25
Recycling cost recovery	**$0.00**
Total cost	**$58.90**

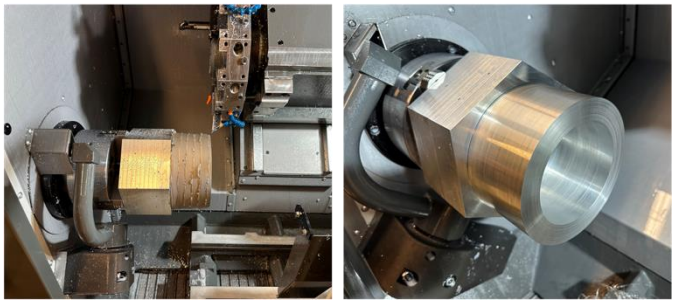

Fig. 9. (Left) preform clamped in the machine spindle prior to turning and (right) after turning operations for both the outside and inside diameters were completed.

3.1.4 Turning

CNC turning was used for the cylindrical section of the preform. A Haas ST-15 CNC lathe was used to machine the outside and inside diameters of the preform. The preform was clamped in the spindle using a three-jaw chuck and the inside surfaces of the hexagon; see Fig. 9. The outside diameter and the front face were turned using a VBMT331 insert (Sandvik 7861072) with a cutting speed of 243.8 m/min and a roughing feed rate of 0.254 mm/rev. The roughing depth of cut was 0.89 mm. A cutting speed of 243.8 m/min and a feed rate of 0.0508 mm/rev were used for the finishing pass. The finish pass depth of cut was 0.13 mm. For the boring operation to machine the internal diameter, a CNGP432 (Kennametal 1785718) insert was used. The same feeds and speeds as well as depths of cut were used to machine the internal geometry of the preform. The finished part geometry is shown in Fig. 9 after the turning operations were completed.

Table 7. Turning cost model variables, values, and units for the hexagon-cylinder.

Variable	Value	Units
C_{mat}	0	$
c_{tool}	20	$
t_{ch}	10	min
C	4200	-
v	243.84	m/min
p	1	-
f_r	0.25	mm/rev
q	1.5	-
V_{rem}	-	mm^3
a	0.89	mm
t_{setup}	60	min
t_{sup}	90	min
r_{lab}	40	$/hr
t_{turn}	90	min
F	1.5	-
$c_{enr\text{-}rate}$	0.12	$/kWh
r_{enr}	14.9	kW
$c_{space,fix}$	75,000	$
$p_{space,fix}$	1	yr
$U_{space,mach}$	19.69	m^2
$U_{space,tot}$	1393	m^2
$c_{equi,I}$	59,195	$
v_{sal}	0	$
L_{exp}	10 years	yr
$c_{maint,p}$	0	$
$c_{maint,t}$	1,000	$
$l_{maint,p}$	0	-
$l_{maint,l}$	1	yr
p_{coll}	0	%

Table 8: Turning cost model summary.

Cost	Value
Direct build costs	**$157.91**
Stock Material cost	$0.00
Tool cost	$26.13
Labor cost	$130.00
Energy cost	$1.79
Indirect build costs	**$2.12**
Space cost	$0.34
Depreciation cost	$1.52
Maintenance cost	$0.26
Recycling cost recovery	**$0.00**
Total cost	**$160.03**

The values for the turning cost model are provided in Table 7. The total cost was $160.02 with significant contributions from both labor and tool costs. The cost summary is given in Table 8.

3.1.5 Total

Combining the costs from the four processes results in a total of $1,007.58. AFSD contributed 61% of the cost. Table 9 lists the costs by manufacturing process. Among cost categories, the largest contributor was labor, which accounted for 65% of the $1007.58. The next largest category was material, which constituted 24% of the total cost; see Table 10.

Table 9. Costs listed by manufacturing process.

Manufacturing process	Estimated cost	% of total
AFSD	$613.32	61%

SLS	$175.34	17%
Milling	$58.90	6%
Turning	$160.04	16%
Total	**$1,007.60**	**100%**

Table 10. Costs listed by spend category.

Category	Cost	% of total
Material	$245.73	24%
Tool	$27.24	3%
Labor	$655.66	65%
Energy	$10.01	1%
Space	$3.01	0%
Depreciation	$58.12	6%
Maintenance	$7.83	1%
Total	**$1,007.60**	**100%**

3.2 Conventional three-axis milling

Using the same milling parameters, machine, and tools selected for the milling portion of the hybrid manufacturing process, tool paths were created to simulate the production of the hexagon-cylinder by three-axis CNC milling from wrought stock with dimensions of 254 mm × 215.9 mm × 228.6 mm (10” × 8.5” × 9”). The machining process plan included two setups. The hexagon was machined in the first setup and the cylinder side was machined in a second setup.

The first setup used an origin set at the bottom center of the wrought stock face. In this orientation, the hexagon top, outside, and interior were machined. The toolpaths are shown in Fig. 10 (left).

The workpiece was inverted for the second setup, so that the top face of the hexagon was in contact with the machine table. In this orientation, the origin was set at the top center as shown in Fig. 10 (right). Using the same tool and parameters as the previous setup, facing and contouring operations were defined to achieve the final external and internal dimensions of the cylinder.

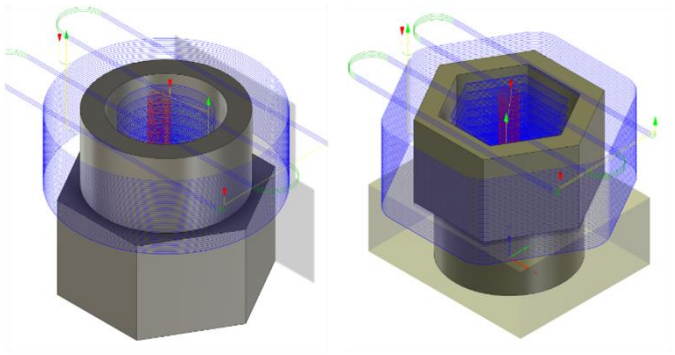

Fig. 10. (Left) The first setup showing milling tool paths to machine the hexagon geometry from wrought stock. (Right) The second setup showing milling tool paths to machine the cylindrical geometry.

Since the same parameters were used to generate the Fig. 10 tool paths, the inputs for the milling cost model remain the same as the hybrid manufacturing setup. The exceptions are milling time, since the entire part is machined from solid wrought stock, and material cost for the solid wrought stock. Using the parameters outlined in Table 11, the cost for producing the part using three-axis milling only is $833.60. The summary is provided in Table 12.

Table 11. Milling cost model variables, values, and units for the hexagon-cylinder (produced by three-axis milling)

Variable	Value	Units
C_{mat}	698	$
c_{tool}	300	$
t_{ch}	10	min
C	17,500	-
v	1224	m/min
n	0.025	-
p	0.015	-
f_t	0.122 mm/min	mm/min
q	0.015	-
V_{rem}	-	mm^3
a	63.5 (-)	mm
b	25	mm
m	4	teeth
N	5115 rpm	rpm
t_{setup}	30 min	min
t_{sup}	104	min
r_{lab}	40	$/hr
t_{mill}	104	min
F	1.5	-
$c_{enr\text{-}rate}$	0.12	$/kWh
r_{enr}	15.5	kW
$c_{space,fix}$	75,000	$
$p_{space,fix}$	year	yr
$U_{space,mach}$	24.71	m^2
$U_{space,tot}$	1393	m^2
$c_{equi,i}$	78,295	$
v_{sal}	0	$
L_{exp}	10 yr	yr
$c_{maint,p}$	0	$
$c_{maint,t}$	2,500	$
$l_{maint,p}$	0	part
$l_{maint,l}$	1 yr	yr
p_{coll}	0	%

Table 12. Conventional milling summary.

Cost	Value
Direct build costs	**$830.14**
Stock material cost	$698.00
Tool cost	$3.30
Labor cost	$124.00
Energy cost	$4.84
Indirect build costs	**$3.46**
Space cost	$0.39
Depreciation cost	$2.33
Maintenance cost	$0.74
Recycling cost recovery	**$0.00**
Total cost	**$833.60**

4. Discussion

For the case study, three-axis milling was less expensive than hybrid manufacturing. Though the hybrid approach reduced material cost by 65%, the conventional method cost $173.98 less. This difference is due to the higher labor costs for hybrid manufacturing. In this case, the hybrid approach is more sensitive to labor rates, while three-axis milling is more sensitive to material cost. As labor rates increase, so will the difference between hybrid and conventional manufacturing methods. However, the cost difference is not the only consideration when selecting the approach.

One aspect not examined here is lead time. Though not captured in this cost model, lead time can be directly related to

costs [57]. For larger parts, such as the hexagon-cylinder, it is often difficult to find a supplier that can source stock material large enough to completely contain the final part and enable the machining-only solution. For example, a regional material supplier was contacted for the required 254 mm × 215.9 mm × 228.6 mm wrought stock, but that size was not available and no quote was provided. In this instance, the machining-only part could not have been produced in the same time frame as the hybrid approach part. Even if a supplier is identified, lead times can still be high. This reduces the amount of product a company can sell, delays projects, and prevents businesses from meeting customer requirements. Hybrid manufacturing reduces lead times that may occur when using conventional approaches.

This case study does not definitively determine whether hybrid manufacturing or conventional approaches are preferable. Because there is variation between machines, company capabilities, geographic location, wage rates, and part requirements, for example, costs can vary significantly. This paper provides a framework for calculating manufacturing costs and identifies which contributions most strongly affect hybrid manufacturing costs. It also provides a basis for comparing hybrid and conventional manufacturing approaches. The MATLAB™ m-files used to calculate the process costs are available for download [58].

Future work will include adding cost models for powder bed fusion, fused filament fabrication, and wire arc additive manufacturing. Additional manufacturing processes cost models such as wire EDM, heat treatment, and water jetting would increase the cost model portfolio. Batching capabilities are another potentially important cost model that could be explored [12].

6. Conclusions

This paper described cost models for additive friction stir deposition, structured light scanning, CNC milling, and CNC turning operations. It implemented the cost models for a hybrid manufacturing case study to produce a hexagon-cylinder part using the four processes. It also provided a comparison between the costs for hybrid manufacturing and conventional (machining-only) approaches. It was observed that the hybrid manufacturing approach was more labor rate-dependent, while the conventional approach was more material cost-dependent.

Acknowledgements

This work was partially supported by the DOE Office of Energy Efficiency and Renewable Energy (EERE), Advanced Manufacturing Office (AMO), under contract DE-AC05-00OR22725. The US government retains and the publisher, by accepting the article for publication, acknowledges that the US government retains a nonexclusive, paid-up, irrevocable, worldwide license to publish or reproduce the published form of this manuscript, or allow others to do so, for US government purposes. DOE will provide public access to these results of federally sponsored research in accordance with the DOE Public Access Plan (http://energy.gov/downloads/doe-public-access-plan). The authors would also like to acknowledge support from the NSF Engineering Research Center for Hybrid Autonomous Manufacturing Moving from Evolution to Revolution (ERC-HAMMER) under Award Number EEC-2133630.

References

[1] Abdoli Bidhandi, R. and Valmohammadi, C., 2017. Effects of supply chain agility on profitability. Business Process Management Journal, 23(5), pp.1064-1082.

[2] Saleeby, K., Feldhausen, T., Love, L. and Kurfess, T., 2020. Rapid retooling for emergency response with hybrid manufacturing. Smart and Sustainable Manufacturing Systems, 4(3).

[3] Zhu, Z., Dhokia, V.G., Nassehi, A. and Newman, S.T., 2013. A review of hybrid manufacturing processes–state of the art and future perspectives. International Journal of Computer Integrated Manufacturing, 26(7), pp.596-615.

[4] Qian, L. and Ben-Arieh, D., 2008. Parametric cost estimation based on activity-based costing: A case study for design and development of rotational parts. International Journal of Production Economics, 113(2), pp.805-818.

[5] Relich, M. and Pawlewski, P., 2018. A case-based reasoning approach to cost estimation of new product development. Neurocomputing, 272, pp.40-45.

[6] Langmaak, S., Wiseall, S., Bru, C., Adkins, R., Scanlan, J. and Sóbester, A., 2013. An activity-based-parametric hybrid cost model to estimate the unit cost of a novel gas turbine component. International Journal of Production Economics, 142(1), pp.74-88.

[7] Scanlan, J., Rao, A., Bru, C., Hale, P. and Marsh, R., 2006. DATUM project: cost estimating environment for support of aerospace design decision making. Journal of aircraft, 43(4), pp.1022-1028.

[8] Spedding, T.A. and Sun, G.Q., 1999. Application of discrete event simulation to the activity based costing of manufacturing systems. International journal of production economics, 58(3), pp.289-301.

[9] Akyol, D.E., Tuncel, G. and Bayhan, G.M., 2005. A comparative analysis of activity-based costing and traditional costing. World Academy of Science, Engineering and Technology, 3(12), pp.44-47.

[10] Hansen, D.R. and Mowen, M.M., 2007. Managerial accounting. South-Western.

[11] J Tah, J.H.M., Thorpe, A. and McCaffer, R., 1994. A survey of indirect cost estimating in practice. Construction management and economics, 12(1), pp.31-36.

[12] Manogharan, G., Wysk, R.A. and Harrysson, O.L., 2016. Additive manufacturing–integrated hybrid manufacturing and subtractive processes: economic model and analysis. International Journal of Computer Integrated Manufacturing, 29(5), pp.473-488.

[13] Strong, D., Kay, M., Conner, B., Wakefield, T. and Manogharan, G., 2018. Hybrid manufacturing–integrating traditional manufacturers with additive manufacturing (AM) supply chain. Additive Manufacturing, 21, pp.159-173.

[14] West, J., Betters, E. and Schmitz, T., 2023. Limited-constraint WAAM fixture for hybrid manufacturing. Manufacturing Letters, 37, pp.66-69.

[15] Wippermann, A., Gutowski, T.G., Denkena, B., Dittrich, M.A. and Wessarges, Y., 2020. Electrical energy and material efficiency analysis of machining, additive and hybrid manufacturing. Journal of Cleaner Production, 251, p.119731.

[16] Lorenz, K.A., Jones, J.B., Wimpenny, D.I. and Jackson, M.R., 2015. A review of hybrid manufacturing. In 2014 International Solid Freeform Fabrication Symposium. University of Texas at Austin.

[17] Schmitz, T., Costa, L., Canfield, B.K., Kincaid, J., Zameroski, R., Garcia, R., Frederick, C., Rossy, A.M. and Moeller, T.M., 2023. Embedded QR code for part authentication in additive friction stir deposition. Manufacturing Letters, 35, pp.16-19.

[18] Kincaid, J., Zameroski, R., Charles, E., No, T., Bohling, J., Compton, B. and Schmitz, T., 2023. Hybrid manufacturing by additive friction stir deposition, metrology, CNC machining, and microstructure analysis. Manufacturing Letters, 35, pp.549-556.

[19] Dvorak, J., Cornelius, A., Corson, G., Zameroski, R., Jacobs, L., Penney, J. and Schmitz, T., 2022. A machining digital twin for hybrid manufacturing. Manufacturing Letters, 33 (Supplement).

[20] Cornelius, A., Dvorak, J., Jacobs, L., Penney, J. and Schmitz, T., 2021. Combination of structured light scanning and external fiducials for coordinate system transfer in hybrid manufacturing. Journal of Manufacturing Processes, 68, pp.1824-1836.

[21] Kincaid, J., Zameroski, R., No, T., Bohling, J., Compton, B. and Schmitz, T., 2023, February. Hybrid Manufacturing: Combining Additive Friction Stir Deposition, Metrology, and Machining. In TMS

Annual Meeting & Exhibition (pp. 3-13). Cham: Springer Nature Switzerland.
[22] Kincaid, J., Charles, E., Garcia, R., Dvorak, J., No, T., Smith, S. and Schmitz, T., 2023. Process planning for hybrid manufacturing using additive friction stir deposition. Manufacturing Letters, 37, pp.26-31.
[23] Dvorak, J., Gilmer, D., Zameroski, R., Cornelius, A. and Schmitz, T., 2023. Freeform Hybrid Manufacturing: Binderjet, Structured Light Scanning, Confocal Microscopy, and CNC Machining. Journal of Manufacturing and Materials Processing, 7(2), p.79.
[24] Schultz, J. P., and Creehan, K., 2010, Friction stir fabrication. USA Patent US8636194B2.
[25] Gray, D.T., 2009. Modeling and characterization of friction stir fabricated coatings on Al6061 and Al5083 substrates (Doctoral dissertation, Virginia Tech).
[26] Kandasamy, K., Renaghan, L.E., Calvert, J.R., Creehan, K.D. and Schultz, J.P., 2013, October. Solid-state additive manufacturing of aluminum and magnesium alloys. In Proceedings of the Materials Science and Technology Conference and Exhibition (p. 59).
[27] Calvert, J.R., 2015. Microstructure and mechanical properties of WE43 alloy produced via additive friction stir technology (Doctoral dissertation, Virginia Tech).
[28] Rivera, O.G., Allison, P.G., Jordon, J.B., Rodriguez, O.L., Brewer, L.N., McClelland, Z., Whittington, W.R., Francis, D., Su, J., Martens, R.L. and Hardwick, N., 2017. Microstructures and mechanical behavior of Inconel 625 fabricated by solid-state additive manufacturing. Materials Science and Engineering: A, 694, pp.1-9.
[29] Tang, W., Yang, X., Tian, C., and Xu, Y., 2022. Microstructural heterogeneity and bonding strength of planar interface formed in additive manufacturing of Al–Mg–Si alloy based on friction and extrusion. International Journal of Minerals, Metallurgy and Materials, 29(9), pp.1755-1769.
[30] Nicholas, E.D., 2003. Friction processing technologies. Welding in the World, 47, pp.2-9.
[31] Hang, Z.Y., Jones, M.E., Brady, G.W., Griffiths, R.J., Garcia, D., Rauch, H.A., Cox, C.D. and Hardwick, N., 2018. Non-beam-based metal additive manufacturing enabled by additive friction stir deposition. Scripta Materialia, 153, pp.122-130.
[32] Beladi, H., Farabi, E., Hodgson, P.D., Barnett, M.R., Rohrer, G.S. and Fabijanic, D., 2022. Microstructure evolution of 316L stainless steel during solid-state additive friction stir deposition. Philosophical Magazine, 102(7), pp.618-633.
[33] Agrawal, P., Haridas, R.S., Yadav, S., Thapliyal, S., Dhal, A. and Mishra, R.S., 2023. Additive friction stir deposition of SS316: Effect of process parameters on microstructure evolution. Materials Characterization, 195, p.112470.
[34] Grasso, M. and Colosimo, B.M., 2017. Process defects and in situ monitoring methods in metal powder bed fusion: a review. Measurement Science and Technology, 28(4), p.044005.
[35] Svetlizky, D., Das, M., Zheng, B., Vyatskikh, A.L., Bose, S., Bandyopadhyay, A., Schoenung, J.M., Lavernia, E.J. and Eliaz, N., 2021. Directed energy deposition (DED) additive manufacturing: Physical characteristics, defects, challenges and applications. Materials Today, 49, pp.271-295.
[36] Perry, M.E., Griffiths, R.J., Garcia, D., Sietins, J.M., Zhu, Y. and Hang, Z.Y., 2020. Morphological and microstructural investigation of the non-planar interface formed in solid-state metal additive manufacturing by additive friction stir deposition. Additive Manufacturing, 35, p.101293.
[37] Ghadimi, H., Ding, H., Emanet, S., Talachian, M., Cox, C., Eller, M. and Guo, S., 2023. Hardness Distribution of Al2050 Parts Fabricated Using Additive Friction Stir Deposition. Materials, 16(3), p.1278.
[38] Rivera, O.G., Allison, P.G., Brewer, L.N., Rodriguez, O.L., Jordon, J.B., Liu, T., Whittington, W.R., Martens, R.L., McClelland, Z., Mason, C.T. and Garcia, L., 2018. Influence of texture and grain refinement on the mechanical behavior of AA2219 fabricated by high shear solid state material deposition. Materials Science and Engineering: A, 724, pp.547-558.
[39] Jordon, J.B., Allison, P.G., Phillips, B.J., Avery, D.Z., Kinser, R.P., Brewer, L.N., Cox, C. and Doherty, K., 2020. Direct recycling of machine chips through a novel solid-state additive manufacturing process. Materials & Design, 193, p.108850.
[40] Phillips, B.J., Avery, D.Z., Liu, T., Rodriguez, O.L., Mason, C.J.T., Jordon, J.B., Brewer, L.N. and Allison, P.G., 2019. Microstructure-deformation relationship of additive friction stir-deposition Al–Mg–Si. Materialia, 7, p.100387.
[41] Babaniaris, S., Jiang, L., Varma, R.K., Farabi, E., Dorin, T., Barnett, M. and Fabijanic, D., 2022. Precipitation in AA6063 produced from swarf using additive friction stir deposition. Additive Manufacturing Letters, 3, p.100096.
[42] Williams, M.B., Cahalan, L.P., Lopez, J.J., Perez-Andrade, L.I., Leonard, R.T., McDonnell, M.M., Kelly, M.R., Lalonde, A.D., Brewer, L.N., Jordon, J.B. and Allison, P.G., 2023. Dynamic Behavior Characterization of Aluminum Alloy 7020 Manufactured Using the Additive Friction Stir Deposition Process. JOM, pp.1-13.
[43] Mason, C.J.T., Rodriguez, R.I., Avery, D.Z., Phillips, B.J., Bernarding, B.P., Williams, M.B., Cobbs, S.D., Jordon, J.B. and Allison, P.G., 2021. Process-structure-property relations for as-deposited solid-state additively manufactured high-strength aluminum alloy. Additive Manufacturing, 40, p.101879.
[44] Yoder, J.K., Griffiths, R.J. and Hang, Z.Y., 2021. Deformation-based additive manufacturing of 7075 aluminum with wrought-like mechanical properties. Materials & Design, 198, p.109288.
[45] Joshi, S.S., Patil, S.M., Mazumder, S., Sharma, S., Riley, D.A., Dowden, S., Banerjee, R. and Dahotre, N.B., 2022. Additive friction stir deposition of AZ31B magnesium alloy. Journal of Magnesium and Alloys, 10(9), pp.2404-2420.
[46] McClelland, Z., Avery, D.Z., Williams, M.B., Mason, C.J.T., Rivera, O.G., Leah, C., Allison, P.G., Jordon, J.B., Martens, R.L. and Hardwick, N., 2019. Microstructure and mechanical properties of high shear material deposition of rare earth magnesium alloys WE43. In Magnesium Technology 2019 (pp. 277-282). Springer International Publishing.
[47] Garcia, D., Hartley, W.D., Rauch, H.A., Griffiths, R.J., Wang, R., Kong, Z.J., Zhu, Y. and Hang, Z.Y., 2020. In situ investigation into temperature evolution and heat generation during additive friction stir deposition: A comparative study of Cu and Al-Mg-Si. Additive Manufacturing, 34, p.101386.
[48] Priedeman, J.L., Phillips, B.J., Lopez, J.J., Tucker Roper, B.E., Hornbuckle, B.C., Darling, K.A., Jordon, J.B., Allison, P.G. and Thompson, G.B., 2020. Microstructure development in additive friction stir-deposited Cu. Metals, 10(11), p.1538.
[49] Avery, D.Z., Rivera, O.G., Mason, C.J.T., Phillips, B.J., Jordon, J.B., Su, J., Hardwick, N. and Allison, P.G., 2018. Fatigue behavior of solid-state additive manufactured inconel 625. Jom, 70, pp.2475-2484.
[50] Griffiths, R.J., Gotawala, N., Hahn, G.D., Garcia, D. and Hang, Z.Y., 2022. Towards underwater additive manufacturing via additive friction stir deposition. Materials & Design, 223, p.111148.
[51] Martin, L.P., Luccitti, A. and Walluk, M., 2022. Evaluation of additive friction stir deposition of AISI 316L for repairing surface material loss in AISI 4340. The International Journal of Advanced Manufacturing Technology, 121(3-4), pp.2365-2381.
[52] Wu, B.L., Peng, Y.C., Tang, H.Q., Meng, C.C., Zhong, Y.F., Zhang, F.L. and Zhan, Y.Z., 2023. Improving grain structure and dispersoid distribution of nanodiamond reinforced AA6061 matrix composite coatings via high-speed additive friction stir deposition. Journal of Materials Processing Technology, p.117983.
[53] Lopez, J.J., Williams, M.B., Rushing, T.W., Confer, M.P., Ghosh, A., Griggs, C.S., Jordon, J.B., Thompson, G.B. and Allison, P.G., 2022. A solid-state additive manufacturing method for aluminum-graphene nanoplatelet composites. Materialia, 23, p.101440.
[54] Griffiths, R.J., Perry, M.E., Sietins, J.M., Zhu, Y., Hardwick, N., Cox, C.D., Rauch, H.A. and Yu, H.Z., 2019. A perspective on solid-state additive manufacturing of aluminum matrix composites using MELD. Journal of Materials Engineering and Performance, 28, pp.648-656.
[55] Rodriguez, R.X., Program Overview: Extra-Large, Metal Additive Manufacturing System, Targeted Towards Army Ground Vehicle Systems. In Proceedings of the Ground Vehicle Systems Engineering and Technology Symposium (pp. 13-15).
[56] Tlusty, J., 2000. Manufacturing Processes and Equipment. (Prentice Hall, NJ).
[57] Karmarkar, U.S., 1993. Manufacturing lead times, order release and capacity loading. Handbooks in operations research and management science, 4, pp.287-329.
[58] https://www.dropbox.com/scl/fi/95j75f6qjkzoo092exn40/MATLAB-cost-models.zip?rlkey=8yd53t173zkh05i60lhwqlb9m&dl=0.